J. Fluid Mech. (2011), *vol.* 687, *pp.* 118–140.
doi:10.1017/jfm.2011.322

Melting and dissolving of a vertical solid surface with laminar compositional convection

Andrew J. Wells†‡ and M. Grae Worster

Institute of Theoretical Geophysics, Department of Applied Mathematics and Theoretical Physics, University of Cambridge, Wilberforce Road, Cambridge CB3 0WA, UK

(Received 15 November 2010; revised 8 June 2011; accepted 23 July 2011; first published online 6 October 2011)

We consider laminar compositional convection of buoyant melt released by ablation of a vertical solid surface into a two-component fluid. Asymptotic solutions are used to describe separate cases: the ablation rate is either controlled by thermal transport, corresponding to melting, or by solutal transport, corresponding to dissolution. Melting is faster and generates a stronger flow than dissolving. We determine the temperature and solute concentration conditions leading to either melting or dissolving and find that these conditions do not vary with the strength of the buoyancy that drives convective flow.

Key words: boundary layer structure, buoyant boundary layers, solidification/melting

1. Introduction

The ablation of a solid in a multi-component melt is of interest in a variety of geophysical, geological and industrial problems. Icebergs float in relatively warm salty water throughout the polar oceans, molten rock rises to fill magma chambers within the earth's crust, and solution mining is used to extract mineral deposits from rock. If ablation of the solid releases melt of different composition into the neighbouring fluid, any resulting difference in density can drive convection within the fluid, which enhances heat and mass transfer from the fluid, and hence the rate of ablation.

As an illustrative example, the rate of ablation of a floating iceberg can be controlled by either the supply of heat or by the supply of salt from the ocean to the ice–water interface. If the supply of heat is large then it controls the ablation rate, and we say that the ice *melts* into the water. Alternatively, if the thermal driving is weaker, salt can build up at the solid–liquid interface and *dissolve* the ice even when the temperature of the ocean is lower than the melting temperature of 0 °C. This distinction was noted for purely diffusive heat and mass transfer by Woods (1992), and the melting and dissolving of a horizontal surface with turbulent convection was studied by Kerr (1994*a*,*b*). Dissolving is of particular interest in the polar oceans, where chemical disequilibrium can generate temperature gradients and heat fluxes that would not be expected by thermal considerations alone. For example, Notz *et al.* (2003) showed that dissolution at the base of sea ice can generate heat transfer from the ice to the ocean, as recently observed in field measurements (Perovich *et al.* 2008).

† Email address for correspondence: Andrew.J.Wells@yale.edu

‡ Present address: Department of Geology and Geophysics, Yale University, New Haven, CT 06520, USA.

There is also evidence that iceberg disintegration is very sensitive to increases in temperature. Morgan & Budd (1978) used iceberg size distributions and drift rates to infer ablation rates of the order of centimetres per day in cool polar waters with temperatures below 0 °C, rising to metres per day in warmer sub-polar waters with temperatures of 5–8 °C. It is not clear to what extent this disintegration is controlled by mechanical fracture or by thermodynamical ablation. It is possible, however, that an increase in temperature may lead to strongly enhanced ablation rates as a result of a transition from slow dissolving to much faster melting.

Whilst turbulent flow will play a role in many geophysical applications, we here focus on laminar flow to build fundamental insight into the interaction of convection and phase change. We consider the ablation of a vertical solid surface in a two-component melt, with laminar compositional convection resulting from the release of buoyant melt. We investigate how laminar convection modifies the dynamics of melting and dissolving from the case of diffusive heat and mass transfer considered by Woods (1992). The results are readily adaptable to the flow of buoyant melt released by ablation under sloping solid surfaces. The analysis of laminar flow also provides fundamental insight for future studies of the more complex turbulent flow that is relevant to icebergs in the ocean. The ablation of an ice surface in warm salty water has previously been considered in studies of both laminar flow (Carey & Gebhart 1982*a*,*b*) and turbulent flow (Josberger & Martin 1981). Carey & Gebhart (1982*a*) found a similarity solution of the boundary-layer equations, that shows behaviour indicative of melting and dissolving, although the authors did not explore this distinction.

In § 2 we explain how the thermodynamic conditions at the interface lead to either melting or dissolving by briefly reviewing the case of phase change where there is no motion in the fluid and the diffusive solution applies (Woods 1992). We then consider the influence of laminar, boundary-layer flow driven by the release of buoyant melt. We focus on the case in which the buoyancy force depends primarily on salinity, and use the separation of scales between diffusion of heat and diffusion of salt to construct matched asymptotic solutions that elucidate the physical structure. The boundary-layer problem is set out in § 3, and scaling is used to indicate the structure of the boundary layer and magnitude of the ablation rate in the separate cases of melting and dissolving. The detailed solutions are derived for melting in § 4 and for dissolving in § 5. In § 6 we consider the conditions that lead to melting or dissolving and compare the two solutions.

2. Diffusive melting and dissolving

In this section we review the distinction between melting and dissolving and how it depends on the thermodynamic conditions at the solid–liquid interface (Woods 1992). A solid of far-field temperature T_s is in contact with a two-component melt of far-field temperature T_∞ and far-field concentration C_∞ at a planar interface $y = a(t)$, as shown in figure 1. The solid has uniform composition C_s. We exemplify the following discussion by considering a fresh water iceberg, of salinity $C_s \approx 0$, in contact with sea water of far-field salinity C_∞, but the analysis is also relevant to other binary melts. The interface temperature T_i and concentration C_i satisfy an equilibrium liquidus constraint $T_i = T_L(C_i)$ for some function $T_L(C)$, which we approximate by the linear relationship

$$T_i = T_L(C_i) \approx T_m - \Gamma(C_i - C_s), \tag{2.1}$$

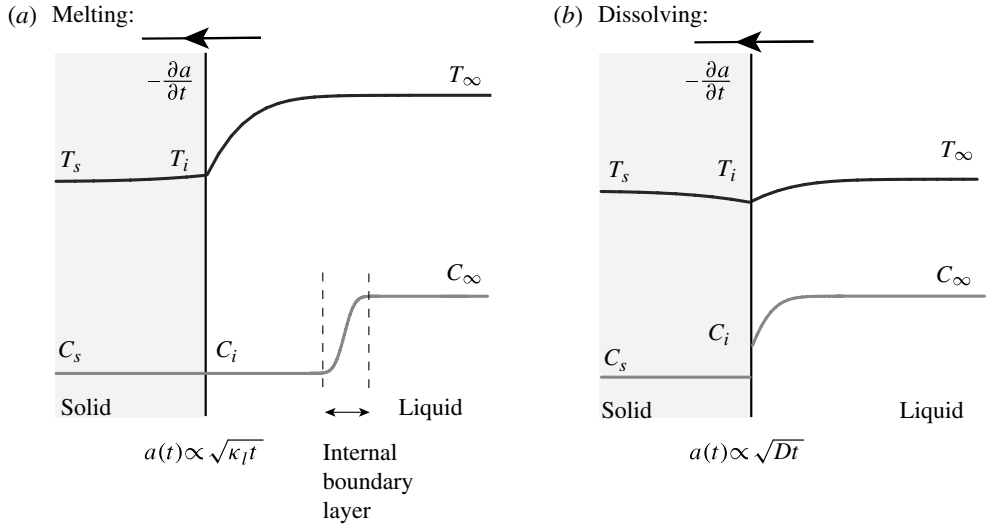

FIGURE 1. Schematic illustration of (*a*) melting and (*b*) dissolving of a solid of concentration C_s and far-field temperature T_s in contact with a two-component melt of far-field concentration C_∞ and far-field temperature T_∞. The solid–liquid interface is located at $y = a(t)$ and has temperature T_i and liquid concentration C_i. In the absence of convection, the rate of ablation is controlled by thermal diffusion for melting and solutal diffusion for dissolving, as described in the text.

where T_m is the melting temperature at concentration C_s, and Γ describes the rate of freezing point depression with increasing concentration. For ice in salty water, $T_m \approx 0$ °C and $\Gamma \approx 0.06$ °C psu^{-1} (Josberger & Martin 1981).

The rate of phase change is determined from heat and salt budgets. Conservation of heat across the solid–liquid interface is expressed by the Stefan condition

$$\rho_s L \frac{\partial a}{\partial t} = \rho_s c_s \kappa_s \left.\frac{\partial T}{\partial y}\right|_{y=a^-} - \rho_l c_l \kappa_l \left.\frac{\partial T}{\partial y}\right|_{y=a^+}, \tag{2.2}$$

where L is the latent heat of fusion and ρ_j, c_j and κ_j are the density, heat capacity and thermal diffusivity of the solid ($j = s$) and liquid ($j = l$) phases. Conservation of solute across the interface is expressed by

$$\rho_s (C_i - C_s) \frac{\partial a}{\partial t} = -\rho_l D \left.\frac{\partial C}{\partial y}\right|_{y=a^+}, \tag{2.3}$$

where D is the solutal diffusivity.

The two conditions (2.2) and (2.3) allow either the heat flux or the salt flux to control the rate of phase change $\dot{a} = \partial a/\partial t$. If the heat supply is large then the heat flux towards the interface controls the ablation rate via the Stefan condition (2.2) and the solid *melts*. For example, Woods (1992) found that when

$$T_\infty - T_m \gtrsim (D/\kappa_l)^{1/2} [T_\infty - T_L(C_\infty)], \tag{2.4}$$

the solid melts at a rate scaling with thermal diffusion, as illustrated in figure 1(*a*). The diffusivity of salt is much smaller than the diffusivity of heat ($D \ll \kappa_l$), so (2.3) shows that $C_i \approx C_s$ in this case. This produces a region of fresh water at the interface, as indicated in figure 1(*a*), with large solutal gradients confined to a narrower 'internal'

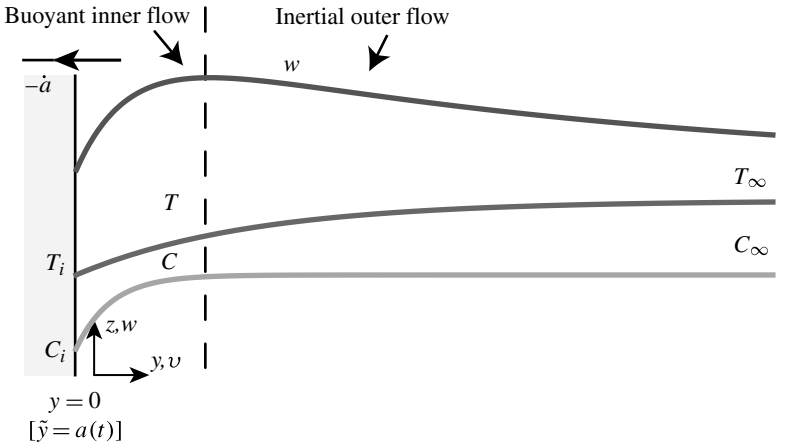

FIGURE 2. A vertical ice surface is in contact with water of uniform far-field temperature T_∞, salinity C_∞ and density ρ_∞. The ablation of ice releases relatively fresh meltwater of density $\rho_l < \rho_\infty$, driving a buoyant meltwater flow upwards with velocity (v, w) in a boundary layer along the surface of the ice. We work in a reference frame in which the interface is stationary at $y = 0$, so that the meltwater released at the interface creates a velocity $v(0)$ relative to the interface. If the molecular viscosity ν is significantly larger than both the thermal diffusivity κ and the solutal diffusivity D, then the flow can be divided into a buoyant, thermal layer close to the interface, and an outer inertial flow as illustrated by the dashed line.

solutal boundary layer located away from the interface. On the other hand, if $T_\infty < T_m$, then the salt flux can control the ablation rate, the solid then *dissolves* into the fluid and there is little release of latent heat. However, the interface temperature is depressed slightly, as shown in figure 1(*b*).

3. Laminar boundary layer flow driven by buoyancy

The density of a binary melt, such as sea water, usually depends strongly on the concentration of solute and so we expect the profiles in figure 1 to generate buoyancy-driven flow that enhances the heat and solute transfer. We focus here on convection at a vertical solid surface in an unstratified fluid. We follow the formulation of Josberger & Martin (1981) and Carey & Gebhart (1982*a*), assuming that the interface remains quasi-planar and vertical (the non-uniform ablation rate changes the slope of the boundary over time, but typically such changes are slow). We work in a reference frame in which the interface is stationary at $y = 0$, as illustrated in figure 2. In this reference frame, we expect the flow to be steady and well described by the incompressible Boussinesq boundary-layer equations. Conservation of mass, momentum, heat and salt are described by

$$\frac{\partial v}{\partial y} + \frac{\partial w}{\partial z} = 0, \tag{3.1}$$

$$v\frac{\partial w}{\partial y} + w\frac{\partial w}{\partial z} = \nu\frac{\partial^2 w}{\partial y^2} - g\left(\rho - \rho_\infty\right)/\rho_l, \tag{3.2}$$

$$v\frac{\partial T}{\partial y} + w\frac{\partial T}{\partial z} = \kappa\frac{\partial^2 T}{\partial y^2}, \tag{3.3}$$

$$v\frac{\partial C}{\partial y} + w\frac{\partial C}{\partial z} = D\frac{\partial^2 C}{\partial y^2}, \tag{3.4}$$

where we have taken the reference density as ρ_l, the density of the liquid at the solid–liquid interface. This system is subject to boundary conditions

$$v = -\frac{\rho_s}{\rho_l}\dot{a}, \quad w = 0, \quad T = T_i, \quad C = C_i \quad \text{at } y = 0, \tag{3.5a,b,c,d}$$

$$T \to T_\infty, \quad C \to C_\infty, \quad w \to 0 \quad \text{as } y \to \infty, \tag{3.5e,f,g}$$

and the thermodynamic conditions (2.1)–(2.3) at the interface. The condition (3.5*a*) imposes a non-zero velocity $v(0)$ relative to the moving interface, owing to a combination of the change in density as ice changes phase into water and the frame advection that results from the interface receding in the rest frame of the ice. This system also describes the flow of buoyant melt under a surface inclined at an angle φ to the horizontal by interpreting z as the distance along the slope and replacing g with the along-slope component of gravity $g\sin\varphi$ (Gebhart *et al.* 1988), provided that the slope angle ϕ is sufficiently steep to avoid flow separation.

Carey & Gebhart (1982*a*) described the density ρ by a nonlinear function of temperature and salinity. We focus on the case of pure compositional convection, using the approximation

$$\rho = \rho_\infty + \rho_l\beta(C - C_\infty). \tag{3.6}$$

This approximation captures the dominant buoyancy driving the flow for ice and sea water systems, where typically the density ratio $(\alpha\Delta T)/(\beta\Delta C) \leqslant 0.05$ for a characteristic temperature scale ΔT, compositional scale ΔC and thermal expansion coefficient α. It also makes the problem more mathematically tractable by neglecting thermal buoyancy and avoiding the possible complication of bi-directional flow, where a fresh upward inner flow is accompanied by a cold outer downward flow (Nilson 1985).

There is no imposed length scale in the problem, and so a solution can be found in terms of a similarity variable

$$\eta = \frac{y}{z}\left(\frac{1}{4}Ra_z\right)^{1/4}, \tag{3.7}$$

which scales the horizontal coordinate y by the characteristic thermal boundary layer thickness for convective flow. We use a local Rayleigh number

$$Ra_z = \frac{g\beta(C_\infty - C_i)z^3}{\kappa_l\nu}, \tag{3.8}$$

that characterizes the ratio of solutal buoyancy to viscous dissipation across the thermal boundary layer.

Incompressibility (3.1) is satisfied by use of a streamfunction ψ such that $v = -\partial\psi/\partial z$ and $w = \partial\psi/\partial y$, and we define a non-dimensional streamfunction f, temperature θ and solute concentration ϕ by

$$\psi = 4\kappa_l\left(\frac{1}{4}Ra_z\right)^{1/4} f(\eta), \quad \theta = \frac{T - T_\infty}{T_i - T_\infty}, \quad \phi = \frac{C - C_\infty}{C_i - C_\infty}, \tag{3.9}$$

so that f' represents the vertical velocity. Note that the interfacial temperature T_i and concentration C_i are unknown *a priori* and are determined from the interfacial thermodynamic conditions. Substituting (3.7)–(3.9) into the boundary layer

equations (3.2)–(3.6) we obtain the coupled ordinary differential equations

$$\sigma^{-1}(2f'^2 - 3ff'') = f''' + \phi \tag{3.10}$$

$$-3f\theta' = \theta'' \tag{3.11}$$

$$-3f\phi' = \epsilon\phi'' \tag{3.12}$$

$$f'(0) = 0, \quad \theta(0) = 1, \quad \phi(0) = 1, \tag{3.13}$$

$$f' \to 0, \quad \theta \to 0, \quad \phi \to 0 \quad \text{as } \eta \to \infty, \tag{3.14}$$

where $\sigma = \nu/\kappa_l$ is the Prandtl number, $\epsilon = 1/Le = D/\kappa_l$ is the inverse of the Lewis number Le and we use primes to denote derivatives with respect to η (e.g. $f' = \mathrm{d}f/\mathrm{d}\eta$).

Ablation releases a fluid flux $f(0)$ relative to the solid–liquid interface, made up of both the blowing velocity that arises if the solid expands when changing phase to a liquid, and the effective advection that results from the solid–liquid interface receding in the rest frame of the solid. The dimensional ablation rate is given by (3.5*a*), which can be expressed as

$$\dot{a} = -\frac{\rho_l}{\rho_s}v(0) = \frac{\rho_l}{\rho_s}3\frac{\kappa_l}{z}\left(\frac{1}{4}Ra_z\right)^{1/4} f(0), \tag{3.15}$$

with $f(0)$ determined from the interface conditions (2.1)–(2.3), which transform to give

$$3f(0) = \left(\frac{1}{\mathscr{S}_T} + \frac{\chi_i}{\mathscr{S}_C}\right)\theta'(0), \tag{3.16}$$

$$3\chi_i f(0) = \epsilon(1 - \chi_i)\phi'(0), \tag{3.17}$$

with $\mathscr{S}_T$, $\mathscr{S}_C$ and χ_i defined below. In the Appendix we show that the heat flux from the solid is typically small, and hence it is neglected here. To clarify the description of transitions between melting and dissolving, the far-field thermal driving and far-field solute conditions are characterized by the Stefan numbers

$$\mathscr{S}_T = \frac{L}{c_l(T_\infty - T_m)}, \quad \mathscr{S}_C = \frac{L}{c_l\Gamma(C_\infty - C_s)}, \tag{3.18}$$

respectively. The total thermal driving on the right-hand side of (3.16) depends on a combination of the sensible heat available in the far field for melting ($1/\mathscr{S}_T$), and the effective amount of heat that could be made available by depression of the freezing point temperature at the far-field salinity ($1/\mathscr{S}_C$). The partitioning of these terms in (3.16) is controlled by the ratio

$$\chi_i = \frac{C_i - C_s}{C_\infty - C_s} = \frac{T_i - T_m}{T_L(C_\infty) - T_m}, \tag{3.19}$$

which characterizes the solute concentration at the interface, and hence the interface temperature as a result of the liquidus relation (2.1). The value of χ_i is determined as part of the solution, with $0 \leqslant \chi_i \leqslant 1$.

Carey & Gebhart (1982*a*) integrated a set of equations similar to (3.10)–(3.19) numerically. We investigate the system asymptotically in order to describe the physical structure of the boundary layer and the distinction between melting and dissolving of the solid.

An interesting feature of the system (3.9)–(3.14) and (3.16)–(3.19) is that the fluid flow is independent of the ratio ρ_s/ρ_l of densities of the solid and liquid phases. One might have expected a significant effect of the blowing velocity for a solid undergoing a large expansion when changing phase to a liquid. However, we find that the velocity

$v(0)$ relative to the interface remains constant as we increase ρ_s/ρ_l, and instead we simply find a reduction in the dimensional ablation rate given by (3.15). This is a consequence of the Stefan condition (2.2) and the condition of mass conservation at the interface (3.5*a*), which can be combined to show that the mass flux of fluid released by ablation is equal to the ratio of the heat flux into the interface and the latent heat per unit mass L required to change phase, independent of the density of the solid.

3.1. *Boundary layer structure*

Further simplification can be obtained in the limit of large Prandtl number and large Lewis number. For example, cold sea water has $\sigma = \nu/\kappa_l \approx 10$ and $Le = \kappa_l/D \approx 200$, so that viscous forces act over a larger length scale than either thermal or solutal diffusion. Kuiken (1968) derived matched asymptotic solutions for the buoyant flow at large Prandtl number next to a fixed heated wall, and Nilson (1985) extended these to two-component convection. As illustrated in figure 2, the temperature and solute variations are confined to an inner layer near to the interface, where buoyancy and viscous forces balance. There is no buoyancy force in the outer region, which is effectively dragged upwards by the buoyant inner flow. The outer solution does not influence the inner layer and always takes the form described by Kuiken (1968). The ablation dynamics are therefore determined by the leading order solution in the inner layer, which is obtained by setting $1/\sigma \approx 0$ in the momentum balance (3.10) to yield

$$f''' + \phi = 0, \tag{3.20}$$

and replacing the far-field boundary conditions (3.14) with

$$f'' \to 0, \quad \theta \to 0, \quad \phi \to 0, \tag{3.21}$$

so that there is zero shear at the outer edge of the inner layer. For a thermal boundary layer, Kuiken (1968) showed that this approximation captures the dominant behaviour for σ as small as 2.

The distinction between melting and dissolving is obtained by considering the further limit of large Lewis number ($Le = \kappa_l/D \gg 1$). As $Le \to \infty$ (or $\epsilon \to 0$) the right-hand side of the solute equation (3.12) becomes small, and so large solutal gradients can only occur in a narrow boundary layer where f is relatively small. Two possibilities are illustrated in figure 3 (to be justified later). If the ablation rate is controlled by a large heat supply, f is large and negative at the interface with strong advection of meltwater away from the interface. The large solutal gradients ϕ' are then confined to a thin, diffusive boundary layer away from the interface where f is close to 0, so that $\boldsymbol{u} \cdot \nabla C \approx 0$ and advection is weak. Hence the diffusive boundary layer is located precisely at the location where there is a transition between the strong net advection of melted fluid away from the ice–water interface ($f < 0$), to inward advection of fluid ($f > 0$) due to boundary layer entrainment beyond the diffusive boundary layer. This is illustrated in figure 3(*a*) and corresponds to melting, with a thermally controlled ablation rate generating a large fresh region close to the interface. The second case (figure 3*b*) corresponds to the solid dissolving, with a smaller ablation rate yielding weak advective transport f and large solutal gradients ϕ' close to the interface, and inward advection of fluid further from the interface.

3.2. *Scalings for the inner layer and ablation rate*

The magnitude of the ablation rate can be determined by considering the scalings in the inner layer for $\epsilon = 1/Le \ll 1$. The buoyancy force is largest at the interface where

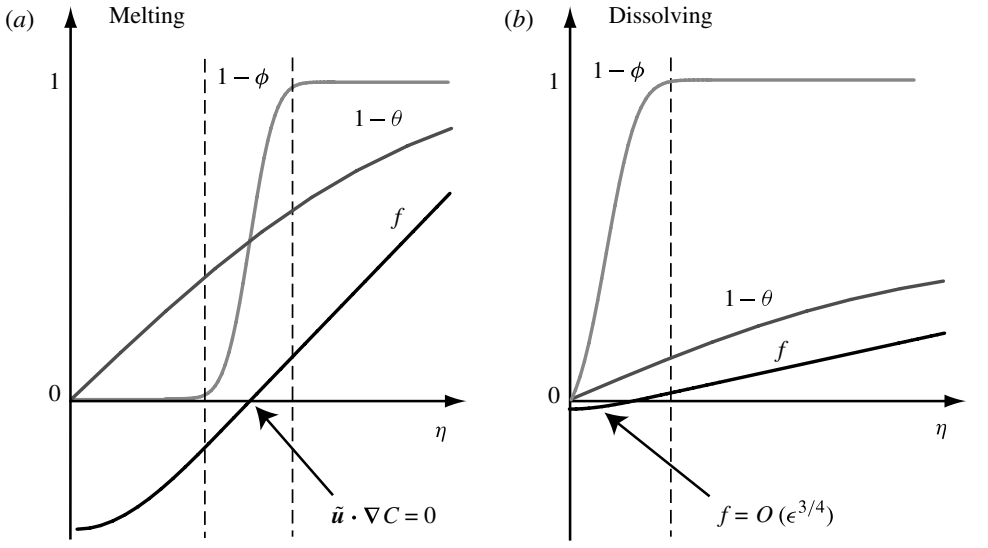

FIGURE 3. Near-wall temperature, concentration and streamfunction profiles, corresponding to the structure within the buoyant, thermal region in figure 2. For large Lewis number the large solutal gradients are confined to a solutal boundary layer in two different cases. (*a*) When the solid is melting, large solute gradients are confined to a thin diffusive boundary layer where the advective transport $f \to 0$, yielding a broad fresh layer close to the interface. (*b*) When the solid is dissolving, the solute gradient ϕ' is large and f is small close to the interface.

the salinity is lowest, and so we always have a balance of buoyancy and viscous forces close to the interface. The heat and solute transfer scalings differ depending on whether the solid is melting or dissolving.

If the heat flux is large then it controls the ablation rate, and we consider scalings where $\theta'(0)$ and $f(0)$ are both $O(1)$. The Stefan condition (3.16) is satisfied by retaining the thermal boundary layer scalings near to the interface, with a large temperature gradient over a boundary layer of width

$$\eta = O(1) \Rightarrow y \sim z\left[\frac{g\beta(C_\infty - C_i)z^3}{\kappa_l \nu}\right]^{-1/4}. \tag{3.22}$$

The dimensional ablation rate is independent of the solutal diffusivity D and given by

$$\frac{\partial a}{\partial t} = \frac{\rho_l c_l (T_\infty - T_i)}{\rho_s L}\frac{\kappa_l}{z}\left[\frac{g\beta(C_\infty - C_i)z^3}{4\kappa_l \nu}\right]^{1/4}\theta'(0). \tag{3.23}$$

It scales with the $1/4$ power of a Rayleigh number based on solutal buoyancy and thermal diffusivity, where $\theta'(0)$ is of order unity. This indicates that the supply of heat controls the width of the region of buoyant fresh meltwater, and hence also controls the strength of the convective flow. The remaining details of the solution for melting are derived in § 4.

The alternative case occurs when the salt flux at the interface is large and controls the ablation rate. The appropriate rescalings are then

$$\eta = \epsilon^{1/4}\xi, \quad f(\eta) = \epsilon^{3/4}F(\xi), \quad \theta(\eta) = \Theta(\xi), \quad \phi(\eta) = \Phi(\xi), \tag{3.24}$$

where F, Θ and Φ are $O(1)$ functions of a rescaled $O(1)$ similarity variable ξ. Setting $1/\sigma = 0$, the inner boundary layer equations (3.11), (3.12) and (3.20) yield

$$F''' + \Phi = 0, \tag{3.25}$$

$$\Theta'' + \epsilon 3F\Theta' = 0, \tag{3.26}$$

$$\Phi'' + 3F\Phi' = 0, \tag{3.27}$$

with interface boundary conditions

$$F'(0) = 0, \quad \Theta(0) = 1, \quad \Phi(0) = 1, \tag{3.28}$$

and the thermodynamic constraints at the interface yield

$$\epsilon 3F(0) = \left(\frac{\chi_i}{\mathscr{S}_C} + \frac{1}{\mathscr{S}_T}\right)\Theta'(0), \tag{3.29}$$

$$3\chi_i F(0) = (1-\chi_i)\,\Phi'(0). \tag{3.30}$$

Note that the rescalings (3.24) have been chosen so that the dimensionless ablation rate $F(0)$ is determined by the salt flux into the interface $\Phi'(0)$ in (3.30).

There are large solutal gradients in a boundary layer next to the interface of width

$$\eta = O(\epsilon^{1/4}) \Rightarrow y \sim z\left[\frac{g\beta(C_\infty - C_i)z^3}{D\nu}\right]^{-1/4}, \tag{3.31}$$

and a dimensional ablation rate

$$\frac{\partial a}{\partial t} = \frac{\rho_l(C_\infty - C_i)}{\rho_s(C_i - C_s)}\frac{D}{z}\left[\frac{g\beta(C_\infty - C_i)z^3}{4D\nu}\right]^{1/4}\Phi'(0), \tag{3.32}$$

where $\Phi'(0) = O(1)$. The ablation rate now scales with the $1/4$ power of a Rayleigh number based on solutal buoyancy and solutal diffusivity, and is independent of the thermal diffusivity κ_l. The scaled Stefan condition (3.29) requires that the heat supply is much weaker, with

$$\left(\frac{1}{\mathscr{S}_T} + \frac{\chi_i}{\mathscr{S}_C}\right)\Theta'(0) = O(\epsilon). \tag{3.33}$$

By comparing (3.23) and (3.32) we immediately see that melting is a large factor, of $O(Le^{3/4})$, faster than dissolving. The remaining details of the solution for dissolving are derived in § 5.

4. Melting solution

When $\theta'(0) = O(1)$ the solid melts into the liquid, thermal boundary layer scalings apply and there is an internal solutal boundary layer. The generic structure of the velocity, temperature and concentration profiles is illustrated in figure 4(*a*).

We first determine the form of the solution in both the inner and outer thermal regions, where the governing equations are given by (3.11), (3.12) and (3.20), and boundary conditions (3.13), (3.16), (3.17) and (3.21). The streamfunction f changes sign across the compositional boundary layer, so we divide the thermal boundary layer into an inner region where $f < 0$ for $\eta < \overline{\eta}$, and an outer region where $f > 0$ for $\eta > \overline{\eta}$, for some $\overline{\eta}$ to be determined. To determine the behaviour for $\epsilon \ll 1$ we seek solutions expanded in powers of $\epsilon^{1/2}$ to allow matching to the internal boundary layer solution considered later. The system (3.11), (3.12) and (3.20) is solved order by order

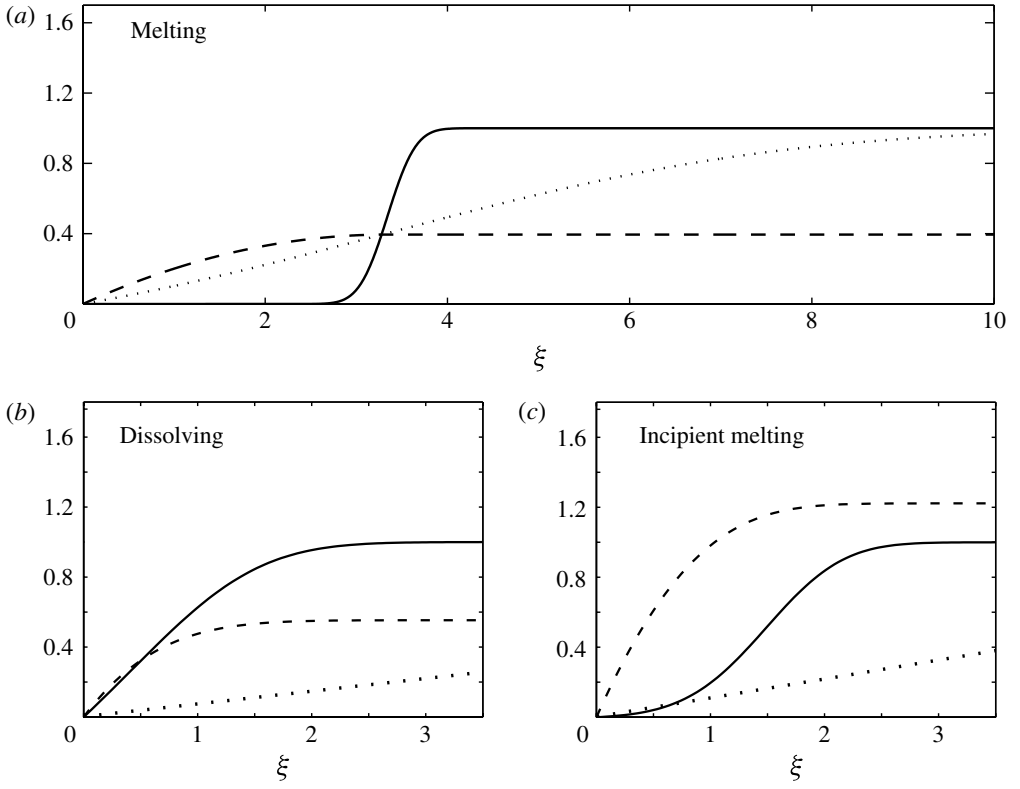

FIGURE 4. Plots of the boundary layer profiles for both melting and dissolving, with $\epsilon = 0.005$. The vertical velocity (f' or F') is shown by a dashed line, the temperature $1 - \Theta$ is shown by a dotted line and the solute profiles $1 - \Phi$ are given by the solid line. Plot (*a*) shows the analytic solution for melting with $1/\mathscr{S}_T = 2$, with the axes scaled in terms of the coordinate $\xi = \eta/\epsilon^{1/4}$ to allow a comparison with the dissolving profiles. Plots (*b*,*c*) show numerical solutions of the inner leading-order ordinary differential equations for dissolving, with domain width $\xi_\infty = 3.5$. The solutions shown for (*b*) $1/\mathscr{S}_T = -0.75$, $1/\mathscr{S}_C = 1$, and (*c*) $1/\mathscr{S}_T = -0.01$, $1/\mathscr{S}_C = 1$ are discussed further in the text. Note that the vertical velocity f' is plotted by a dashed curve in (*a*), with $f' = F'/\epsilon^{1/2}$. Hence, the absolute velocity for melting in (*a*) is actually asymptotically larger than the velocity for dissolving in (*b*,*c*), even though both f' and F' are $O(1)$ in the figures. The supply of heat is larger for (*c*) than for (*b*), and we observe a transition to incipient melting behaviour.

in increasing powers of $\epsilon^{1/2}$. The solutal balance (3.12) shows $\phi' = 0$ at all orders whenever $\eta \neq \overline{\eta}$, so that the solute gradient is exponentially small across both the inner and outer thermal regions. Applying the interface boundary condition $\phi(0) = 1$ and far-field boundary condition $\phi(\infty) = 0$ to the appropriate regions we obtain

$$\phi = 1, \quad \eta < \overline{\eta} \quad \text{and} \quad \phi = 0, \quad \eta > \overline{\eta}. \tag{4.1a,b}$$

The leading order solute concentration changes discontinuously at $\eta = \overline{\eta}$, with an almost fresh region with dimensional salinity $C \approx C_s$ confined close to the interface, changing abruptly to the far-field salinity $C = C_\infty$ in a region further from the wall.

Noting that the solute gradient $\phi'(0)$ is exponentially small, the condition (3.17) of solute conservation at the interface requires that the concentration ratio

$$\chi_i = 0 \tag{4.2}$$

at all orders if ablation is to occur with $f(0) = O(1)$. This implies that the interface salinity is almost identical to that of the solid (i.e. $C_i \approx C_s$), and hence the interfacial temperature is very close to the freshwater melting point ($T_i \approx T_m$).

The momentum balance (3.20) can be combined with (4.1*a*,*b*) and integrated to yield the streamfunction

$$f = \tfrac{1}{6}\overline{\eta}^3 - \tfrac{1}{2}f''(0)\overline{\eta}^2 + \tfrac{1}{2}f''(0)\eta^2 - \tfrac{1}{6}\eta^3, \quad \eta < \overline{\eta}, \tag{4.3}$$

$$f = f'(\infty)(\eta - \overline{\eta}), \quad \eta > \overline{\eta}. \tag{4.4}$$

The boundary conditions $f'(0) = 0$ and $f''(\infty) = 0$ have been applied here, corresponding to a no-slip condition at the interface and zero shear in the far field, and we have used the fact that $f(\overline{\eta}) = 0$ by definition, to simplify the constants of integration. The buoyancy force is confined to the inner region $\eta < \overline{\eta}$ and drives the flow according to (4.3). There is no buoyancy in the outer region, and so (4.4) shows that the vertical velocity f' remains constant across this outer layer.

The heat equation (3.11) is integrated, using the streamfunction profiles (4.3) and (4.4), to yield

$$\theta = 1 + \theta'(0)\int_0^{\eta} \exp\left\{\tfrac{1}{8}x^4 - \tfrac{1}{2}f''(0)x^3 - \left[\tfrac{1}{2}\overline{\eta}^3 - \tfrac{3}{2}f''(0)\overline{\eta}^2\right]x\right\}\mathrm{d}x, \quad \eta < \overline{\eta}, \tag{4.5}$$

$$\theta = -\theta'(\overline{\eta})\sqrt{\frac{\pi}{6f'(\infty)}}\,\mathrm{erfc}\left[\sqrt{\frac{3f'(\infty)}{2}}(\eta - \overline{\eta})\right], \quad \eta > \overline{\eta}, \tag{4.6}$$

with the temperature θ decaying to its far-field value in the outer thermal layer. We have applied the boundary conditions $\theta(0) = 1$ and $\theta(\infty) = 0$ here, and the constants $\theta'(0)$ and $\theta'(\overline{\eta})$ are to be determined by asymptotic matching via the solution in the internal compositional boundary layer. The complementary error function is defined by

$$\mathrm{erfc}\,[X] = \frac{2}{\sqrt{\pi}}\int_X^{\infty} \exp[-x^2]\,\mathrm{d}x, \tag{4.7}$$

and for small X can be approximated by

$$\mathrm{erfc}\,[X] \sim 1 - \frac{2}{\sqrt{\pi}}X + O(X^2) \quad \text{as } X \to 0. \tag{4.8}$$

The next stage of the calculation is to solve for the profiles within the internal solutal boundary layer, which match the inner and outer solutions. The key difference from the solutal boundary layer for dissolving, described in § 3.2 and considered later in § 5, is that because the solutal variation occurs away from the interface the buoyancy force need not be comparable to the viscous forces. The inner layer scaling breaks down when the advection of salt is weak and comparable to solutal diffusion so that $\epsilon\phi'' \sim f\phi'$ and now $f \to 0$. As we approach this internal boundary layer, the streamfunction is linear at leading order with

$$f(\eta) \sim f'(\overline{\eta})(\eta - \overline{\eta}) \quad \text{as } \eta \to \overline{\eta}. \tag{4.9}$$

Balancing advection and diffusion of salt in (3.12) requires the rescaling

$$\eta - \overline{\eta} = \epsilon^{1/2}\zeta, \quad f(\eta) = \epsilon^{1/2}F(\zeta), \quad \phi(\eta) = \Phi(\zeta), \quad \theta(\eta) = \Theta(\zeta), \tag{4.10}$$

so that the full set of governing equations for the internal boundary layer are

$$F''' + \epsilon\Phi = 0, \tag{4.11}$$

$$\Theta'' + \epsilon 3F\Theta' = 0, \tag{4.12}$$

$$\Phi'' + 3F\Phi' = 0. \tag{4.13}$$

The boundary conditions come from matching to the inner and outer solutions at the edges of the internal boundary layer.

The buoyancy force is weak and of $O(\epsilon)$ in the momentum balance (4.11), and hence integrating (4.11) three times and matching to the outer streamfunction f using $\lim_{\eta\to\overline{\eta}_+} f(\eta) = \lim_{\zeta\to\infty} \epsilon^{1/2} F(\zeta)$ yields

$$F = f'(\infty)\zeta + O(\epsilon), \tag{4.14}$$

so that the vertical velocity F' is approximately constant at leading order in the internal boundary layer. Matching (4.14) to the inner streamfunction f given by (4.3) requires that $\lim_{\eta\to\overline{\eta}_-} f(\eta) = \lim_{\zeta\to-\infty} \epsilon^{1/2} F(\zeta)$, yielding

$$f''(0) = \eta_0 + O(\epsilon^{1/2}), \quad f'(\infty) = \tfrac{1}{2}\eta_0^2 + O(\epsilon^{1/2}), \tag{4.15}$$

after a little algebra, where $\overline{\eta} = \eta_0 + O(\epsilon^{1/2})$ is determined later from the interface conditions.

Writing $\Phi = \Phi_0 + O(\epsilon^{1/2})$, the solute balance (4.13), reduces to the leading order form

$$\Phi_0'' + \tfrac{3}{2}\eta_0^2\zeta\Phi_0' = 0, \tag{4.16}$$

using (4.14) and (4.15), with boundary conditions

$$\Phi_0 \to 1 \quad \text{as } \zeta \to -\infty \quad \text{and} \quad \Phi_0 \to 0 \quad \text{as } \zeta \to \infty \tag{4.17}$$

given by matching to (4.1*a*,*b*). The solution is

$$\Phi_0 = \frac{1}{2}\operatorname{erfc}\left[\frac{\sqrt{3}\eta_0\zeta}{2}\right], \tag{4.18}$$

so that the jump in solute concentration is smoothed out by an error-function decay across the solutal boundary layer.

For $\epsilon \ll 1$ the heat equation (4.12) integrates to give

$$\Theta = \Theta(0) + \Theta'(0)\zeta + O(\epsilon). \tag{4.19}$$

Matching to the inner and outer temperature profiles (4.5) and (4.6), requires $\lim_{\eta\to\overline{\eta}_-} \theta(\eta) = \lim_{\zeta\to-\infty} \Theta(\zeta)$ and $\lim_{\eta\to\overline{\eta}_+} \theta(\eta) = \lim_{\zeta\to\infty} \Theta(\zeta)$, respectively, and after some algebra we obtain all constants of integration in terms of η_0, with the solution summarized in table 1.

The remaining constant η_0 is determined from the Stefan condition (3.16), which simplifies using $\chi_i = 0$ to yield the condition

$$g(\eta_0) \equiv \eta_0^3 \left\{ \int_0^{\eta_0} \exp\left[\frac{1}{8}x^4 - \frac{1}{2}\eta_0 x^3 + \eta_0^3 x\right] \mathrm{d}x + \frac{1}{\eta_0}\sqrt{\frac{\pi}{3}} \exp\left[\frac{5}{8}\eta_0^4\right] \right\} = \frac{1}{\mathscr{S}_T}. \tag{4.32}$$

The value of η_0 depends only on the strength of the far-field thermal driving $1/\mathscr{S}_T$, and hence the profiles of all non-dimensional variables are independent of the far-field salinity. Note that $g(0) = 0$, and $g(x) \to \infty$ as $x \to \infty$ so that a solution η_0 always exists for $1/\mathscr{S}_T > 0$.

Typical concentration, velocity and temperature profiles for melting are illustrated in figure 4(*a*), for $1/\mathscr{S}_T = 2$ and $\epsilon = 0.005$. The salinity shows a large fresh region

Inner thermal:

$$\theta = 1 - \mathscr{S}_T \eta_0^3 \int_0^\eta \exp\left[\frac{1}{8}x^4 - \frac{1}{2}\eta_0 x^3 + \eta_0^3 x\right] \mathrm{d}x + O(\epsilon^{1/2}), \tag{4.20}$$

$$\phi = 1, \tag{4.21}$$

$$f = -\frac{1}{3}\eta_0^3 + \frac{1}{2}\eta_0\eta^2 - \frac{1}{6}\eta^3 + O(\epsilon^{1/2}). \tag{4.22}$$

Internal solutal:

$$\Theta = \mathscr{S}_T \eta_0^2 \sqrt{\frac{\pi}{3}} \exp\left[\frac{5}{8}\eta_0^4\right] + O(\epsilon^{1/2}), \tag{4.23}$$

$$\Phi = \frac{1}{2}\mathrm{erfc}\left[\frac{\sqrt{3}\eta_0\zeta}{2}\right] + O(\epsilon^{1/2}), \tag{4.24}$$

$$F = \frac{1}{2}\eta_0^2\zeta + O(\epsilon^{1/2}). \tag{4.25}$$

$$\zeta = \frac{\eta - \eta_0}{\epsilon^{1/2}}, \quad f(\eta) = \epsilon^{1/2}F(\zeta), \quad \theta(\eta) = \Theta(\zeta), \quad \phi(\eta) = \Phi(\zeta). \tag{4.26}$$

Outer thermal:

$$\theta = \mathscr{S}_T \eta_0^2 \sqrt{\frac{\pi}{3}} \exp\left[\frac{5}{8}\eta_0^4\right] \mathrm{erfc}\left[\frac{\sqrt{3}\eta_0(\eta - \eta_0)}{2}\right] + O(\epsilon^{1/2}), \tag{4.27}$$

$$\phi = 0, \tag{4.28}$$

$$f = \frac{1}{2}\eta_0^2(\eta - \eta_0) + O(\epsilon^{1/2}). \tag{4.29}$$

Interface:

$$f(0) = -\frac{1}{3}\eta_0^3 + O(\epsilon^{1/2}), \tag{4.30}$$

$$\frac{1}{\mathscr{S}_T} = \eta_0^3 \left\{ \int_0^{\eta_0} \exp\left[\frac{1}{8}x^4 - \frac{1}{2}\eta_0 x^3 + \eta_0^3 x\right] \mathrm{d}x + \frac{1}{\eta_0}\sqrt{\frac{\pi}{3}} \exp\left[\frac{5}{8}\eta_0^4\right] \right\}. \tag{4.31}$$

TABLE 1. The leading order asymptotic solutions for the case of melting. The thermal boundary layer is split into inner and outer regions, joined by an internal solutal boundary layer for $\zeta = (\eta - \eta_0)/\epsilon^{1/2} = O(1)$. The value of η_0 is determined by the condition (4.31) in terms of the thermal Stefan number $\mathscr{S}_T$.

with negligible solutal gradient close to the interface, followed by a rapid decay to the far-field salinity across the narrow internal solutal boundary layer. The vertical velocity increases with distance from the interface in the inner thermal layer, where the solute concentration is relatively fresh and buoyancy is significant, before remaining approximately constant in the outer thermal region, where there is no buoyancy. The temperature decays slowly across the entire width of the inner and outer thermal layers.

The interface conditions determine when the ice is melting and the solution (4.20)–(4.31) can be applied. Firstly, the equation (4.31) for η_0 only has positive solutions for $\mathscr{S}_T > 0$, and hence we need $T_\infty > T_m$. The Stefan condition (3.16) requires $1/\mathscr{S}_T \gg \epsilon^{1/2}$ as a result of the scaling ansatz that $f(0) \gg \epsilon^{1/2}$ and $\theta'(0) \gg \epsilon^{1/2}$. The melting solution is therefore valid whenever

$$\frac{c_l(T_\infty - T_m)}{L} \gg \epsilon^{1/2}, \tag{4.33}$$

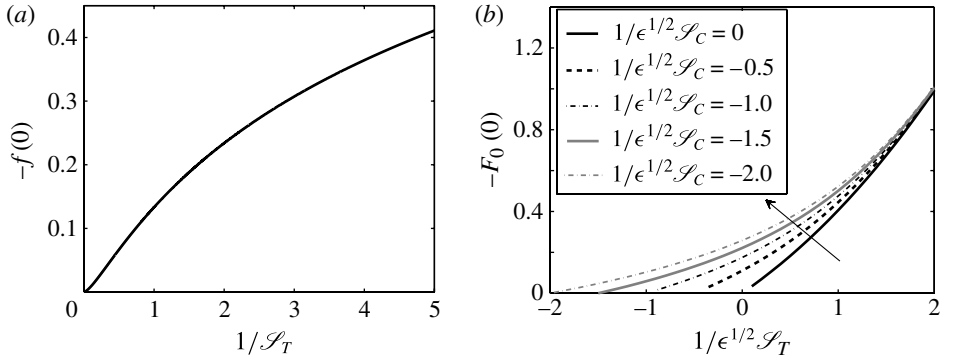

FIGURE 5. Plot (a) shows the variation of non-dimensional melt rate $-f(0)$ as a function of non-dimensional far-field temperature $1/\mathscr{S}_T = c_l(T_\infty - T_m)/L$, for the melting solution. Plot (b) shows the scaled ablation rate $F_0(0) = \epsilon^{3/4} f(0)$ for dissolving and its variation with far-field temperature $1/\epsilon^{1/2}\mathscr{S}_T$ for a variety of salinities given by different values of $1/\epsilon^{1/2}\mathscr{S}_C$. The ablation rate for dissolving increases with salinity for cold temperatures with $\mathscr{S}_T < 0$ (as indicated by the arrow, which shows the direction of increasing $-1/\epsilon^{1/2}\mathscr{S}_C$) and approaches a uniform curve independent of salinity for larger temperatures with $\mathscr{S}_T > 0$.

so that melting occurs whenever the far-field temperature is sufficiently larger than the freshwater melting point. Note that the condition (4.33) is entirely independent of the salinity of the fluid.

The non-dimensional ablation rate is given by $f(0)$ according to (4.30), with $f < 0$ for ablation. Figure 5(a) shows the variation of the magnitude of the ablation rate with scaled far-field temperature $1/\mathscr{S}_T$, with the region $1/\mathscr{S}_T \gg \epsilon^{1/2}$ corresponding to melting. The melt rate $-f(0)$ increases as the thermal driving $1/\mathscr{S}_T$ increases, but the rate of change of $-f(0)$ with $1/\mathscr{S}_T$ slows for larger $1/\mathscr{S}_T$. This behaviour is consistent with the larger temperature difference being partially compensated for by a wider region of fresh meltwater at the interface which slows the increase in the temperature gradient, and hence partially offsets the increase in heat flux to the interface. Note that typically $|1/\mathscr{S}_T| < 0.02$ for ice melting in the polar oceans, and so the saturation of the ablation rate at large values of $1/\mathscr{S}_T$ is not relevant to the ocean, but can be relevant in geological systems where it is possible to find $1/\mathscr{S}_T \approx 2$ for a basaltic magma intrusion that is ∼440 °C hotter than the surrounding rock (Kerr 1994*a*).

5. Dissolving solution

We now derive the detailed asymptotic solution for ice dissolving, showing that buoyancy is confined within the inner boundary layer with large solutal gradients, described by (3.24)–(3.30). There is also an outer thermal layer where there is constant salinity and velocity, and the temperature adjusts to its far-field value. We consider the outer layer first, which provides far-field boundary conditions for the inner layer.

The outer layer is characterized by a balance between advection and diffusion of heat, which suggests the rescaling

$$\xi = \epsilon^{-1/2}\mathscr{Y}, \quad F = \epsilon^{-1/2}\mathscr{F}(\mathscr{Y}), \quad \Theta = \mathscr{T}(\mathscr{Y}), \quad \Phi = \mathscr{P}(\mathscr{Y}), \tag{5.1}$$

where the rescaled streamfunction $\mathscr{F}$, temperature $\mathscr{T}$ and salinity $\mathscr{P}$ are all order-one functions of the rescaled coordinate $\mathscr{Y}$. The governing equations for the outer layer

are

$$\mathscr{F}''' + \epsilon \mathscr{P} = 0, \tag{5.2}$$

$$\mathscr{T}'' + 3\mathscr{F}\mathscr{T}' = 0, \tag{5.3}$$

$$\epsilon \mathscr{P}'' + 3\mathscr{F}\mathscr{P}' = 0. \tag{5.4}$$

The far-field boundary conditions (3.21) yield

$$\mathscr{F}'' \to 0, \quad \mathscr{T} \to 0, \quad \mathscr{P} \to 0 \quad \text{as } \mathscr{Y} \to \infty, \tag{5.5}$$

with additional boundary conditions to be determined by matching to the inner solution. Note that the outer velocity $f' = \epsilon^{1/2}\mathscr{F}' = O(\epsilon^{1/2})$ is relatively weak in the case of dissolving because the velocity is generated by buoyancy confined to the narrow solutal boundary layer next to the interface.

In order to match the inner layer scalings we seek solutions expanded in powers of $\epsilon^{1/4}$. If $\mathscr{F} \neq 0$ in the outer layer, and $\mathscr{P} = \sum_{n=0}^{\infty} \mathscr{P}_n(\mathscr{Y})\epsilon^{n/4}$, then the solute equation (5.4) requires that all of the $\mathscr{P}_n' \equiv 0$ throughout the outer layer, and the far-field boundary conditions result in

$$\mathscr{P} \equiv 0, \tag{5.6}$$

at all orders. This means that there is no buoyancy in the outer layer, and the outer momentum balance (5.2) has solutions of the form

$$\mathscr{F} = \mathscr{F}(0) + \mathscr{F}'(0)\mathscr{Y}, \tag{5.7}$$

where we have used the boundary condition $\mathscr{F}''(\infty) = 0$. Hence, the vertical velocity $\mathscr{F}'$ is constant across the outer layer. The constants $\mathscr{F}(0)$ and $\mathscr{F}'(0)$ are determined by matching to the inner flow, with the condition $\lim_{\mathscr{Y}\to 0} \epsilon^{1/4}\mathscr{F}(\mathscr{Y}) = \lim_{\xi\to\infty} \epsilon^{3/4}F(\xi)$ leading to the boundary condition

$$F_0''(\infty) = 0, \tag{5.8}$$

on the inner solution, and an outer streamfunction

$$\mathscr{F} = F_0'(\infty)\mathscr{Y} + O\left(\epsilon^{1/4}\right), \tag{5.9}$$

where $F_0'(\infty)$ will be determined later from the inner solution.

Using (5.9) the heat equation (5.3) integrates to give the temperature profile

$$\mathscr{T}(\mathscr{Y}) = \mathscr{T}(0)\mathrm{erfc}\left[\sqrt{\frac{3F_0'(\infty)}{2}}\mathscr{Y}\right]\{1 + O(\epsilon^{1/4})\} \tag{5.10}$$

where one constant of integration has been chosen to satisfy the far-field boundary condition $\mathscr{T}(\infty) = 0$, and $\mathscr{T}(0)$ will be found by matching to the inner solution.

With the form of the outer solution determined, we now return to the inner layer which is described by the scalings (3.24) and governing equations (3.25)–(3.30). The far-field boundary conditions are obtained from matching to the outer layer, yielding (5.8), $\Phi(\infty) = 0$ and an additional condition from matching the temperature solutions. Seeking solutions expanded in powers of $\epsilon^{1/4}$, the heat equation (3.26) integrates to yield the temperature profile

$$\Theta(\xi) = 1 + \Theta'(0)\xi + O(\epsilon), \tag{5.11}$$

where we have applied the interface temperature boundary condition $\Theta(0) = 1$. Matching $\lim_{\mathscr{Y}\to 0} \mathscr{T}(\mathscr{Y}) = \lim_{\xi\to\infty} \Theta(\xi)$ yields $\mathscr{T}(0) = 1$ and

$$\Theta'(0) = -\epsilon^{1/2}\left[\frac{6F_0'(\infty)}{\pi}\right]^{1/2} + O(\epsilon^{3/4}). \tag{5.12}$$

The temperature gradient is relatively weak at the interface and throughout the inner layer, with $\Theta'(0) = O(\epsilon^{1/2})$.

The leading order streamfunction F_0 and solute concentration Φ_0 for the inner layer satisfy the fifth order system of coupled ordinary differential equations,

$$F_0''' + \Phi_0 = 0, \tag{5.13}$$

$$\Phi_0'' + 3F_0\Phi_0' = 0, \tag{5.14}$$

subject to the boundary conditions

$$F_0'(0) = 0, \quad \Phi_0(0) = 1, \quad F_0''(\infty) = 0, \quad \Phi_0(\infty) = 0, \tag{5.15}$$

from the interface conditions (3.28) and matching to the outer solution. The final boundary condition comes from the coupled thermodynamic conditions (3.29) and (3.30) at the interface, which can be used to determine the range of far-field temperatures and salinities that lead to dissolving.

Using the temperature gradient (5.12), the Stefan condition (3.29) requires that

$$\chi_i = -\frac{\mathscr{S}_C}{\mathscr{S}_T} - 3\epsilon^{1/2}\mathscr{S}_C F_0(0)\left[\frac{\pi}{6F_0'(\infty)}\right]^{1/2} + O(\epsilon^{3/4}\mathscr{S}_C). \tag{5.16}$$

The solute condition (3.30) must be satisfied with $F(0)$ and $\Phi'(0)$ both of $O(1)$, and hence we also require that $\chi_i = O(1)$, so that there is a build up of salt at the interface and depression of the interface temperature. This can be achieved in two possible ways.

If $\epsilon^{1/2}\mathscr{S}_C = O(\epsilon^{1/4})$, then we have a relatively large supply of solute and (5.16) gives

$$\chi_i = -\frac{\mathscr{S}_C}{\mathscr{S}_T} + O(\epsilon^{1/4}). \tag{5.17}$$

Noting that interface ablation occurs when $F(0) < 0$ and hence requires $0 < \chi_i < 1$, the condition (5.17) can be used to show that we obtain a dissolving solution when

$$T_\infty < T_m, \quad \frac{c_l\Gamma(C_\infty - C_S)}{L} \gg \epsilon^{1/2} \quad \text{and} \quad 1 > \frac{T_m - T_\infty}{T_m - T_L(C_\infty)} \gg \epsilon^{1/4}. \tag{5.18}$$

The second case occurs if both $1/\mathscr{S}_C = O(\epsilon^{1/2})$ and $1/\mathscr{S}_T = O(\epsilon^{1/2})$, so that the supply of heat and solute are both relatively small. We then require that

$$\chi_i = -\frac{\mathscr{S}_C}{\mathscr{S}_T} - 3\epsilon^{1/2}\mathscr{S}_C F_0(0)\left[\frac{\pi}{6F_0'(\infty)}\right]^{1/2} + O(\epsilon^{1/4}), \tag{5.19}$$

with $F_0(0)$ and $F_0'(\infty)$ given by the numerical solution of the inner governing differential equations. Returning to dimensional variables, this requires

$$\frac{c_l(T_\infty - T_m)}{L} = O(\epsilon^{1/2}), \quad \frac{c_l\Gamma(C_\infty - C_S)}{L} = O(\epsilon^{1/2}) \quad \text{and} \quad \frac{T_m - T_i}{T_m - T_L(C_\infty)} \gg \epsilon^{1/4}, \tag{5.20}$$

Inner solutal:

$$\Theta = 1 - \epsilon^{1/2}\left[\frac{6F_0'(\infty)}{\pi}\right]^{1/2}\xi + O(\epsilon^{3/4}), \tag{5.21}$$

$$F_0''' + \Phi_0 = 0, \quad \Phi_0'' + 3F_0\Phi_0' = 0, \tag{5.22}$$

$$F_0'(0) = 0, \quad \Phi_0(0) = 1, \quad F_0''(\infty) = \Phi_0(\infty) = 0 \tag{5.23}$$

$$3\chi_i F_0(0) = (1-\chi_i)\Phi_0'(0), \tag{5.24}$$

$$\chi_i = -\frac{\mathscr{S}_C}{\mathscr{S}_T} - 3\epsilon^{1/2}\mathscr{S}_C F_0(0)\left[\frac{\pi}{6F_0'(\infty)}\right]^{1/2} + O(\epsilon^{3/4}\mathscr{S}_C). \tag{5.25}$$

Outer thermal:

$$\mathscr{T} = \operatorname{erfc}\left[\sqrt{\frac{3F_0'(\infty)}{2}}\mathscr{Y}\right]\{1 + O(\epsilon^{1/4})\}, \tag{5.26}$$

$$\mathscr{P} \equiv 0, \tag{5.27}$$

$$\mathscr{F} = F_0'(\infty)\mathscr{Y} + O(\epsilon^{1/4}). \tag{5.28}$$

Scalings:

$$f(\eta) = \epsilon^{3/4}F(\xi), \quad \theta(\eta) = \Theta(\xi), \quad \phi(\eta) = \Phi(\xi), \quad \eta = \epsilon^{1/4}\xi. \tag{5.29}$$

$$f(\eta) = \epsilon^{1/4}\mathscr{F}(\mathscr{Y}), \quad \theta(\eta) = \mathscr{T}(\mathscr{Y}), \quad \phi(\eta) = \mathscr{P}(\mathscr{Y}), \quad \eta = \epsilon^{-1/4}\mathscr{Y}. \tag{5.30}$$

TABLE 2. The inner and outer leading order asymptotic solutions for the case of dissolving. The inner streamfunction F_0 and solute concentration Φ_0 are determined by a numerical integration of the system (5.22)–(5.25).

where the exact value of T_i is evaluated by numerical solution of the inner differential equations. Note that we can have $T_\infty > T_m$ in this regime.

The complete leading order solution for the case of dissolving is summarized in table 2. The leading order streamfunction F_0 and solute concentration Φ_0 were determined by a numerical integration of the boundary value problem (5.22)–(5.25) using a modified shooting method (see Acton 1990, for more details of the standard shooting procedure). A comparison (not shown here) of the asymptotic solutions to the corresponding numerical solutions of Carey & Gebhart (1982*a*) and the experimental data of Josberger & Martin (1981) and Carey & Gebhart (1982*b*) shows good qualitative agreement, with all errors smaller than the asymptotic error bounds.

Figure 4(*b*,*c*) shows a selection of inner layer solutions for different values of $\mathscr{S}_T$ and $\mathscr{S}_C$, corresponding to different far-field temperatures and salinities. Cases (*b*) and (*c*) correspond to the limit (5.18), with the far-field temperature less than the fresh water melting point ($T_\infty < T_m$). In (*b*), $1/\mathscr{S}_T = -0.75$, $1/\mathscr{S}_C = 1$ and the solute profile shows an exponential-like decay across the width of the inner boundary layer. The vertical velocity grows monotonically and saturates at a constant value at the edge of the inner layer. Case (*c*) shows the solution as T_∞ approaches T_m, with $1/\mathscr{S}_T = -0.01$ and $1/\mathscr{S}_C = 1$. We begin to see a transition to melting like behaviour, with the magnitude of the solutal gradient initially increasing as we move away from the interface, before decaying in the far field. The non-dimensional interface concentration is $\chi_i = 0.01$ here, so that the interface is fairly fresh and we are moving beyond the domain of validity for the dissolving solution.

Figure 5(*b*) illustrates the variation of the ablation rate $-F_0(0)$ with far-field temperature for the case of weaker solutal driving described by (5.20). The ablation

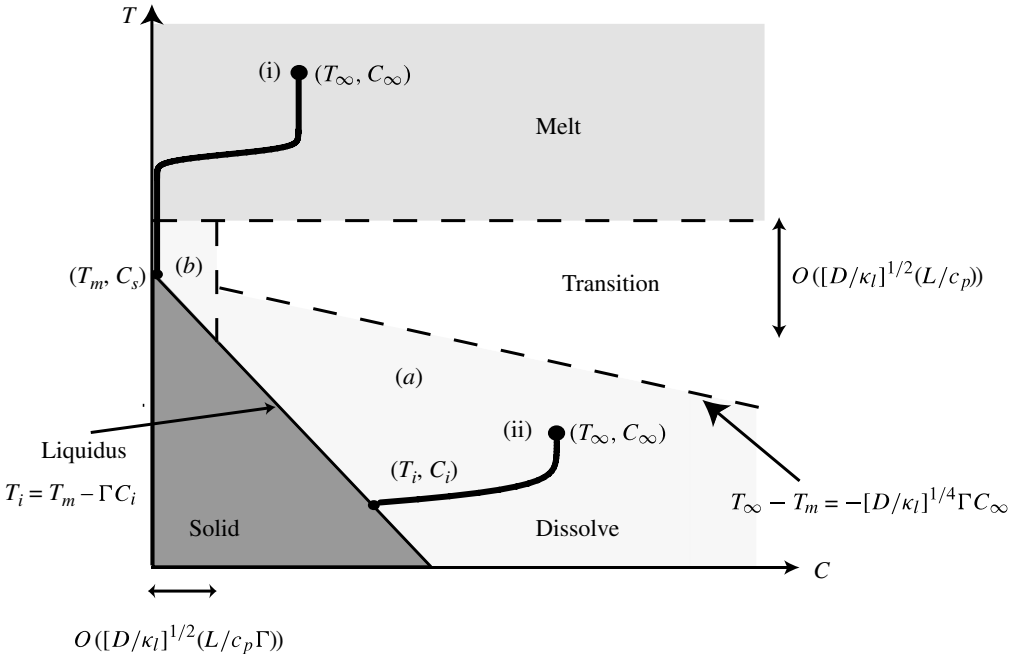

FIGURE 6. Schematic illustration of regions of melting and dissolving behaviour in the (C_∞, T_∞) plane. The solid black line corresponds to the liquidus curve $T = T_L(C)$, and dashed lines indicate regime boundaries. Melting occurs for far-field temperatures sufficiently larger than the freshwater melting point with $T_\infty - T_m \gg (D/\kappa_l)^{1/2}L/c_l$. Dissolving occurs for far-field temperatures lower than the freshwater melting point, in the region (a) with $T_m - T_\infty \gg (D/\kappa_l)^{1/2}L/c_l$ and $T_\infty < T_m$. The dissolving scalings are still valid in an intermediate transition region (b) with $T_\infty - T_m = O([D/\kappa_l]^{1/2}L/c_l)$, although the solutions begin to approach melting-like behaviour for $T_\infty > T_m$. Also shown are two possible trajectories in the phase plane, tracing the changes in temperature and salinity of the boundary layer profiles as we move from the far field with temperature T_∞ and salinity C_∞ into the interface at $T_i = T_L(C_i)$, for (i) melting and (ii) dissolving.

rate depends strongly on the far-field salinity for temperatures less than the fresh water melting point ($\mathscr{S}_T < 0$), consistent with the ice dissolving controlled by solutal transport. For larger temperatures ($\mathscr{S}_T > 0$), the non-dimensional ablation rate curves converge to a single curve that is independent of salinity, consistent with the incipient melting behaviour observed in the boundary layer profiles in figure 4(*c*).

6. Discussion

We now compare the solutions for dissolving and melting. The transition between dissolving and melting depends on the far-field temperature and salinity, with asymptotic conditions for the occurrence of dissolving given by (5.18)–(5.20) and of melting given by (4.33). The resulting asymptotic boundaries are illustrated in a (C_∞, T_∞) phase plane plot in figure 6. We see that the changeover between melting and dissolving occurs when

$$\frac{1}{\mathscr{S}_T} = \frac{c_l(T_\infty - T_m)}{L} = O\left(\left[\frac{D}{\kappa_l}\right]^{1/2}\right) \tag{6.1}$$

Transport mechanism	Vertical velocity	Ablation rate	Solutal boundary layer width	Thermal boundary layer width
Laminar convection	$O(\epsilon^{1/2})$	$O(\epsilon^{3/4})$	$O(\epsilon^{1/4})$	$O(\epsilon^{-1/4})$
Diffusion	—	$O(\epsilon^{1/2})$	$O(\epsilon^{1/2})$	$O(1)$

TABLE 3. Relative magnitude of the dissolving solution properties compared with the melting solution for each of the vertical velocity, ablation rate, solutal boundary layer width and thermal boundary layer width. Each table entry shows the ratio of the dissolving scaling divided by the melting scaling, so that the corresponding velocities, ablation rates and boundary layer widths would be $O(1)$ for melting. The inverse Lewis number is $\epsilon = D/\kappa_l \ll 1$. The differences between transport by laminar convection and transport by molecular diffusion without fluid flow (Woods 1992) are discussed in the text.

which is the same as the criterion found by Kerr (1994*a*) for turbulent convection at a horizontal surface. The condition (6.1) requires a relatively large change in temperature for systems with a large ratio of latent and specific heats. For example, an iceberg in the ocean would require a temperature change of about 5 °C to exceed (6.1). The changeover may be more significant in geological systems, where temperature differences are significantly larger. For the igneous intrusions considered by Kerr (1994*b*), the changeover between melting and dissolving can be achieved with temperature changes of only 1 °C. This is small compared with the temperature differences of order 100 °C or more that are often found in such geological settings.

An interesting feature of the transition criteria (5.18)–(5.20) and (4.33) is that all conditions are entirely independent of the reduced gravity of the flow $g' = g\beta(C_\infty - C_s)$, so that the strength of the buoyancy force has no effect on the conditions for melting and dissolving. Furthermore, (6.1) shows that the transition criterion scales with $(D/\kappa_l)^{1/2}$, similar to the diffusive solution of Woods (1992). A possible explanation for this transition criterion being independent of buoyancy is as follows. The boundary-layer equations (3.3)–(3.4) show that advection balances diffusion for the transport of both heat and salt, and that the advection of fluid influences both heat and solute transport in the same fashion. Therefore, any change in ratio of solutal and thermal transport requires a switch in dominance between solutal and thermal diffusion, and we recover the diffusive scaling $(D/\kappa_l)^{1/2}$ for transition, independent of g' and the strength of the advective flow. Laminar convection does not alter when melting or dissolving occur, but merely modifies the scalings of the boundary layer profiles and resulting ablation rates as compared with the diffusive case. Table 3 compares the ratio of scalings for dissolving and melting, as discussed below.

For the case of dissolving, there is a solutal boundary layer at the interface of width

$$y \sim z\left[\frac{g\beta(C_\infty - C_i)z^3}{D\nu}\right]^{-1/4}, \tag{6.2}$$

nested in a wider thermal boundary layer of width

$$y \sim \left(\frac{\kappa_l}{D}\right)^{1/2} z\left[\frac{g\beta(C_\infty - C_i)z^3}{D\nu}\right]^{-1/4}. \tag{6.3}$$

The ratio of solutal and thermal boundary layer thicknesses is $O([D/\kappa_l]^{1/2})$ for dissolving with laminar convection, which also matches the scaling obtained for diffusive melting and dissolving (Woods 1992), consistent with the reasoning outlined above.

The vertical velocity for dissolving scales as

$$w \sim \frac{4D}{z}\left[\frac{g\beta(C_\infty - C_i)z^3}{4D\nu}\right]^{1/2}, \tag{6.4}$$

depending on a Rayleigh number based on solutal buoyancy and solutal diffusion. This reflects the fact that, when dissolving, the salt supply controls the ablation rate and hence the supply of fresh melt water, which in turn provides the buoyancy to drive the flow. The ablation rate

$$\frac{\partial a}{\partial t} = \frac{(C_\infty - C_i)}{(C_i - C_s)}\frac{D}{z}\left[\frac{g\beta(C_\infty - C_i)z^3}{4D\nu}\right]^{1/4}\Phi'(0), \tag{6.5}$$

is relatively weak because it is controlled by solutal transport, and also scales with a Rayleigh number based on solutal diffusion.

For melting we find a larger solutal boundary layer width, a larger velocity and a larger ablation rate because everything is controlled by the more efficient thermal transport. The solute concentration has a relatively fresh region at the interface, with the width of this region scaling with the thermal boundary layer thickness,

$$y \sim z\left[\frac{g\beta(C_\infty - C_i)z^3}{\kappa_l\nu}\right]^{-1/4}. \tag{6.6}$$

This provides a wide source of buoyancy, so that the vertical velocity

$$w \sim O\left(\frac{4\kappa_l}{z}\left[\frac{g\beta(C_\infty - C_s)z^3}{4\kappa_l\nu}\right]^{1/2}\right), \tag{6.7}$$

is $O([\kappa_l/D]^{1/2})$ larger for melting than the corresponding scaling (6.4) for dissolving. The enhanced convective transport also contributes to a larger melting rate,

$$\frac{\partial a}{\partial t} = 3\frac{\rho_l}{\rho_s}\frac{c_l(T_\infty - T_i)}{L}\frac{\kappa_l}{z}\left[\frac{g\beta(C_\infty - C_s)z^3}{4\kappa_l\nu}\right]^{1/4}\theta'(0), \tag{6.8}$$

where $\theta'(0) = O(1)$. The melting rate (6.8) is $O([\kappa_l/D]^{3/4})$ larger than the ablation rate (6.5) for dissolving, and this will mean the vertical mass flux is also $O([\kappa_l/D]^{3/4})$ larger for melting. Note that both the velocity and the ablation rate for melting scale with a Rayleigh number based on thermal transport and solutal buoyancy. This recognizes the role of the heat supply in controlling the release of fresh meltwater at the interface, and thereby determining the strength of the resulting buoyancy force.

In the melting case, the main variation in salinity occurs in an internal solutal boundary layer, away from the interface. This boundary layer occurs about the point where $f \to 0$, and hence $\boldsymbol{u}\cdot\nabla C \to 0$ and $\boldsymbol{u}\cdot\nabla T \to 0$, so that advection is comparatively small. The internal boundary layer is therefore of a diffusive nature, consistent with its width being $O([D/\kappa_l]^{1/2})$ times the thermal boundary layer width. The widths of the thermal boundary layer, and also the region of large solutal gradients are both narrower for melting than for dissolving, with melting generating a larger velocity and more efficient transport via advection.

It is also interesting to compare the magnitude of the ablation rates predicted for convective and diffusive heat and mass transfer. The advection of heat and salt generated by a convective flow greatly enhances the heat and salt transport into the interface, and the laminar convective flow therefore has significantly larger ablation rates. For example, for a 5 cm block of ice in sea water with $T_\infty = 2\ ^\circ\mathrm{C}$ and $C_\infty = 35$ psu, (6.8) predicts a depth averaged melt rate $\dot{a} \approx 15$ cm day^{-1}. For purely diffusive ablation, with no convection, the ice block would only melt by 2 mm in one day. In addition, the difference in ablation rates between melting and dissolving is more pronounced with laminar convection, scaling as $O([\kappa_l/D]^{3/4})$ as compared with $O([\kappa_l/D]^{1/2})$ for diffusive ablation. We note that convection is likely to have even greater importance in both large-scale oceanic problems and geological magma intrusions, where the flow will be turbulent over most of the solid surface, and will significantly enhance the transport of heat and solute. A full quantification of melting and dissolving in these applications will require an extension of the ideas presented here to account for turbulent convection at vertical and sloping solid surfaces, and whether the resulting solutal and thermal boundary layer structures create bidirectional flow with a fresh buoyant inner flow accompanied by an opposing flow of colder dense liquid.

7. Summary

We have considered the ablation of a vertical solid surface in a binary solution resulting from the heat and salt transfer due to laminar convection of buoyant melt released at the interface. An asymptotic analysis has elucidated differences between melting, where the ablation rate is controlled by thermal transport, and dissolving, where solutal transport controls the ablation rate. A surprising result is that the increase in temperature required for a transition from dissolving to melting does not change significantly from the criterion for purely diffusive heat and mass transfer. In particular, this criterion is entirely independent of the reduced gravity, which characterizes the strength of the buoyancy-driven convection. This is despite differences in boundary layer profiles and ablation rates between the cases of pure diffusion and laminar convective flow.

For dissolving with convection, there is a narrow solutal boundary layer, a weak buoyancy force and hence weak flow, and also a slow ablation rate. All of these properties are controlled by a balance between advection and solutal diffusion, as reflected by scalings dependent on a purely solutal Rayleigh number. By comparison, the ablation rate is thermally controlled for melting, generating a wide region of fresh fluid near to the solid surface and hence stronger flow and larger ablation rates. The flow dynamics are controlled by a balance between advection and thermal diffusion when the solid melts. We also find that the enhanced convective transport yields larger ablation rates than diffusive transport, and the ablation rates, velocities and boundary layer thicknesses all vary with height. These interactions between convection and melting or dissolving may provide insight for the development of models of the melting of icebergs and Antarctic ice shelves, or melting and dissolution in geological applications which feature turbulent convective flows.

Appendix. Heat transfer in the solid phase

A full solution of the Stefan condition (2.2) requires the heat transfer q_s from the solid into the interface. However, we can show that q_s can be neglected at leading order for ablation with large Stefan number, as is typical in the polar oceans.

In the rest frame of the ice, heat transfer is described by the unsteady diffusion equation

$$\dot{T} = \kappa_s \nabla^2 T, \quad \tilde{y} < a. \tag{A 1}$$

This equation simplifies considerably by transforming to the reference frame with $y = \tilde{y} - a$, where the solid–liquid interface remains stationary and quasi-vertical, yielding

$$-\dot{a}\frac{\partial T}{\partial y} = \kappa_s \frac{\partial^2 T}{\partial y^2}, \quad y < 0. \tag{A 2}$$

We have assumed here that the transfer of heat is quasi-steady and depends only weakly on z at leading order. The temperature is fixed in the interior of the solid and at the interface, yielding boundary conditions

$$T \to T_s \quad \text{as } y \to -\infty, \quad T = T_i \quad \text{at } y = 0. \tag{A 3}$$

The system (A 2)–(A 3) has a solution

$$T = T_s + (T_i - T_s)\exp\left[-\dot{a}\frac{y}{\kappa_s}\right], \tag{A 4}$$

so that the heat flux from the solid into the interface $y = 0$ is given by

$$q_s = -\rho_s c_s \kappa_s \left.\frac{\partial T}{\partial y}\right|_{y=0} = \rho_s c_s (T_i - T_s)\dot{a}. \tag{A 5}$$

Recalling from (2.2) that the Stefan condition is

$$\rho_s L\dot{a} = q_l - q_s, \tag{A 6}$$

we see that the heat flux q_s described by (A 5) will play a negligible role whenever the temperature conditions in the solid yield a large Stefan number

$$\frac{L}{c_s\,(T_i - T_s)} \gg 1. \tag{A 7}$$

We expect the condition (A 7) to be satisfied for most situations in the polar oceans. The heat flux q_s from the solid can therefore be neglected to simplify the analysis, but could alternatively be reintroduced in a straightforward fashion by replacing the latent heat L by $L + c_s(T_i - T_s)$ throughout the analysis.

REFERENCES

ACTON, F. S. 1990 *Numerical Methods that Work*. MAA.

CAREY, V. P. & GEBHART, B. 1982*a* Transport near a vertical ice surface melting in saline water: some numerical calculations. *J. Fluid Mech.* **117**, 379–402.

CAREY, V. P. & GEBHART, B. 1982*b* Transport near a vertical ice surface melting in saline water: experiments at low salinities. *J. Fluid Mech.* **117**, 403–423.

GEBHART, B., JALURIA, Y., MAHAJAN, R. L. & SAMMAKIA, B. 1988 *Buoyancy Induced Flows and Transport*, pp. 547–655 Hemisphere, ch. 11.

JOSBERGER, E. G. & MARTIN, S. 1981 A laboratory and theoretical study of the boundary layer adjacent to a vertical melting ice wall in salt water. *J. Fluid Mech.* **111**, 439–473.

KERR, R. C. 1994*a* Melting driven by vigorous compositional convection. *J. Fluid Mech.* **280**, 255–285.

KERR, R. C. 1994*b* Dissolving driven by vigorous compositional convection. *J. Fluid Mech.* **280**, 287–302.

KUIKEN, H. K. 1968 An asymptotic solution for large Prandtl number free convection. *J. Engng Maths* **2** (4), 355–371.

MORGAN, V. I. & BUDD, W. F. 1978 The distribution, movement and melt rates of Antarctic icebergs. In *Iceberg Utilization: Proceedings of the First International Conference.* (ed. A. Husseiny). pp. 220–228. Pergamon Press.

NILSON, R. H. 1985 Countercurrent convection in a double diffusive boundary layer. *J. Fluid Mech.* **160**, 181–210.

NOTZ, D., MCPHEE, M. G., WORSTER, M. G., MAYKUT, G. A., SCHLÜNZEN, K. H. & EICKEN, H. 2003 Impact of underwater–ice evolution on Arctic summer sea ice. *J. Geophys. Res.* **108**, 16–1–16–12.

PEROVICH, D. K., RICHTER-MENGE, J. A., JONES, K. F. & LIGHT, B. 2008 Sunlight, water and ice: extreme arctic sea ice melt during the summer of 2007. *Geophys. Res. Lett.* **35**, doi:10.1029/2008GL034007.

WOODS, A. W. 1992 Melting and dissolving. *J. Fluid Mech.* **239**, 429–448.